Observed multi-decadal increase in the surface ocean's thermal inertia

Hajoon Song (hajsong@yonsei.ac.kr)
Yonsei University https://orcid.org/0000-0003-1895-9124
Chaehyeong Lee
Yonsei University https://orcid.org/0009-0005-3110-9839
Yeonju Choi
Yonsei University
Ajin Cho
Yonsei University
John Marshall
Massachusetts Institute of Technology

Physical Sciences - Article

Keywords: sea surface temperature, memory timescale, climate change, mixed layer, stratification, marine heatwaves

Posted Date: January 12th, 2024

DOI: https://doi.org/10.21203/rs.3.rs-3834500/v1

Additional Declarations: There is **NO** Competing Interest.

Observed multi-decadal increase in the surface ocean's thermal inertia

Chaehyeong Lee[1], Hajoon Song[1,2*†], Yeonju Choi[1], Ajin Cho[1], John Marshall[3]

[1]Department of Atmospheric Sciences, Yonsei University, 50 Yonsei-ro Seodaemun-gu, Seoul, Republic of Korea.
[2]Division of Environmental Science & Engineering, Pohang University of Science and Technology, 77, Cheongam-ro, Nam-gu, Pohang, Republic of Korea.
[3]Department of Earth, Atmospheric and Planetary Sciences, Massachusetts Institute of Technology, 77 Massachusetts Ave. Cambridge, USA.

*Corresponding author(s). E-mail(s): hajsong@yonsei.ac.kr;
Contributing authors: lch204ok@yonsei.ac.kr; ywn0709@yonsei.ac.kr; ajin05@yonsei.ac.kr; jmarsh@mit.edu;
†These authors contributed equally to this work.

Keywords: sea surface temperature, memory timescale, climate change, mixed layer, stratification, marine heatwaves

The ocean surface layer plays a pivotal role in Earth's climate by absorbing excess heat from the atmosphere, thereby regulating global temperatures. Here we document an observed and very notable increase in the persistence of sea surface temperature around the global ocean over the past four decades. This prolonged memory is attributed to two key factors: a

deepening of the surface mixed layer and a decrease in the damping rates due to processes such as vertical entrainment, mixing and damping to the atmosphere. Our findings have great relevance to the observed increase in the duration of marine heatwaves and associated heightened thermal threats to marine organisms. Our study also suggests that the ocean's ability to sequester heat is weakening, a trend that may accelerate as the 21st century proceeds.

Sea surface temperature (SST) has an intrinsic tendency to relax back to its prior state when perturbed often by atmospheric forcing (Frankignoul and Hasselmann, 1977; Deser et al., 2010; Xie, 1999). This negative feedback mitigates positive SST anomalies through loss of energy to the atmosphere or storage within the ocean's interior. The damping rate of near-surface ocean thermal anomalies controls, for instance, the threat posed by thermal stress on marine life (Frölicher and Laufkötter, 2018; Mills et al., 2013; Moore et al., 2012). The potential for the ocean to buffer climate change is also affected, of great import because more than 90% of the Earth's excess energy due to greenhouse gas emissions has been drawn down into its interior (Rhein et al., 2013; Trenberth et al., 2014; Von Schuckmann et al., 2023).

The response of SST to anomalies in forcing can be portrayed by a simple first-order auto-regressive (AR(1)) process (Frankignoul and Hasselmann, 1977), whereby anomalies decay exponentially over time. This simple model aptly captures the observed "red noise" power spectrum of SST. The ocean's mixed layer integrates stochastic atmospheric forcing, characterized by a "white noise" spectrum, yielding a dampened SST variability at shorter timescales (less than 1 year) (Hasselmann, 1976; Frankignoul and Hasselmann, 1977; Marshall and Plumb, 2008; Deser et al., 2010; Boulton and Lenton, 2015; Patrizio and Thompson, 2022). According to this framework, the decay rate of SST anomalies depends on the heat capacity of the mixed layer and the efficiency of the negative feedback (damping) processes. The deepening of the mixed layer and a weakening of damping rates can extend the persistence of the SST anomalies. While prolonged SST persistence leads to enhanced predictability, it also intensifies the potential threat of thermal anomalies to marine ecosystems, perhaps resulting in mortality and shifts in species composition ((Smale et al., 2019) and references therein). For all these reasons, quantifying changes in SST persistence is of great importance.

The persistence of SST and its associated memory timescale have been examined using both observations and numerical models. North Pacific decadal changes in the monthly mean SST memory timescale have been found, due to both large-scale variability and local cloud-SST positive feedback (Ding and Li, 2009). Monthly SST anomalies in the North Pacific tend to persist for longer, associated with a deepening trend in the mixed layer, potentially posing a significant risk to marine ecosystems (Boulton and Lenton, 2015). The same trend in the monthly SST anomalies in the North Pacific and Atlantic is attributed to the weakening of negative feedback processes (Lenton et al., 2017). Projections from earth system models suggest an anticipated decline in long-term SST memory under the Shared Socioeconomic Pathway SSP5-8.5 scenario for the 21st century, resulting from the shoaling of surface mixed layer depth (MLD) driven by global surface warming (Shi et al., 2022).

The persistence of SST on timescales shorter than one month is a crucial area of investigation. The duration of marine heatwaves (MHWs), defined as an event with positive SST anomalies exceeding the 90th percentile and lasting for at least five consecutive days (Hobday et al., 2016, 2018), shows a tight correlation with the daily SST memory timescale (Oliver et al., 2021). In eastern boundary upwelling regions, synoptic scale winds drive variations in SST on timescales of a few days, impacting nutrient distribution and primary productivity through coastal upwelling (Botsford et al., 2006; García-Reyes et al., 2014; Aguirre et al., 2014, 2019). Additionally, marine species are sensitive to both mean temperatures and to variabilities occurring over days to weeks (Dillon et al., 2016).

The trend in daily SST memory timescales may diverge from that of monthly SST due to the influence of rapidly varying processes such as surface waves and the submesoscale (Bulgin et al., 2020). Indeed, the projected daily surface temperature persistence increase in the 21st century contradicts the anticipated decreasing trend in annual-scale SST anomalies (Li and Thompson, 2021; Shi et al., 2022). In this study, the daily SST memory timescale was evaluated using 40 years of satellite data, which was not previously reported. We find a statistically significant increase of daily SST memory timescale across the major part of the global ocean, potentially associated with the deepening trend of the mixed layer.

The observed memory timescale of SST and its decadal trend

To estimate the memory timescale of SST, the daily quarter-degree resolution NOAA Optimum Interpolation SST dataset (Reynolds et al., 2007) is fitted to the AR(1) model for each year (see Methods) to find the damping coefficient (λ in (1)). Our approach is equivalent to finding the time at which the lag 1-day autocorrelation coefficient falls below $1/e$, as in Oliver et al. (2021). We find that, typically, daily SST memory timescales are shorter than 30 days, except in the eastern equatorial Pacific where they exceed 50 days (Fig. 1a). Other regions with long memory timescales include the eastern North Pacific, the regions north of the Gulf Stream and Kuroshio current, the Agulhas Retroflection and the eastern South Indian Ocean. In contrast, the equatorial western Pacific, Indian, Atlantic and much of the Southern Oceans have memory timescales shorter than 10 days.

The daily SST memory trend timescale exhibits a statistically significant increase over the global ocean almost everywhere (Fig. 1b). The most rapid increases are found

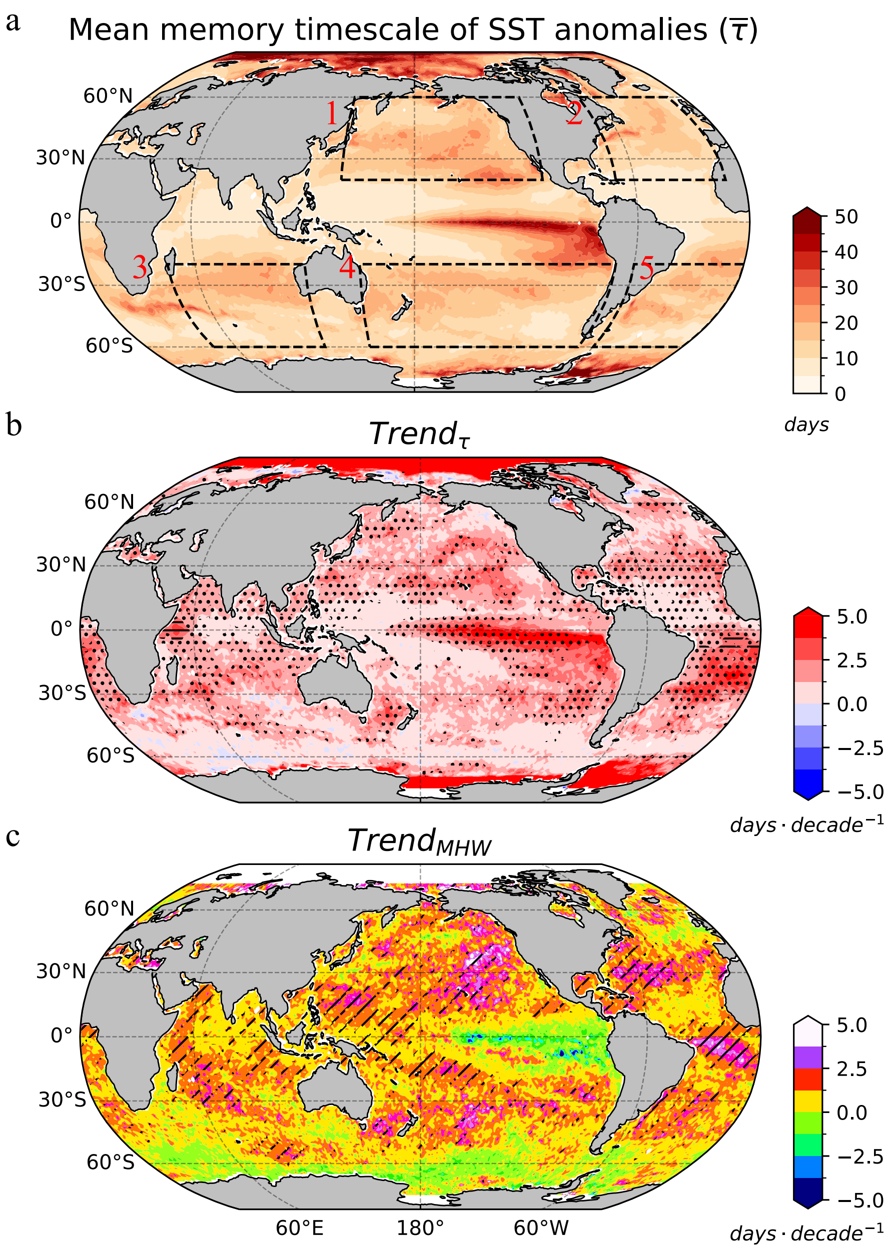

Fig. 1 **a**. The mean memory timescale of the SST anomalies ($\overline{\tau}$) estimated from the observation. **b**. The linear trend from 1982 to 2021. The black boxes in **a** indicate the regions where the energy spectra of the SST anomalies were calculated. Box numbers 1 through 5 represent North Pacific, North Atlantic, Indian Ocean, South Pacific, and South Atlantic, respectively. The dotted and dashed areas in **b** represent the regions where τ in 2021 has increased by 50-100% and over 100% compared to 1982, respectively. Note that nearly every region globally exhibits a statistically significant increasing trend. **c**. Linear trend in the duration of marine heatwaves from 1982 to 2021. The dashed areas in **c** represent the regions in which trends in marine heatwaves duration are statistically significant at the 95% confidence level.

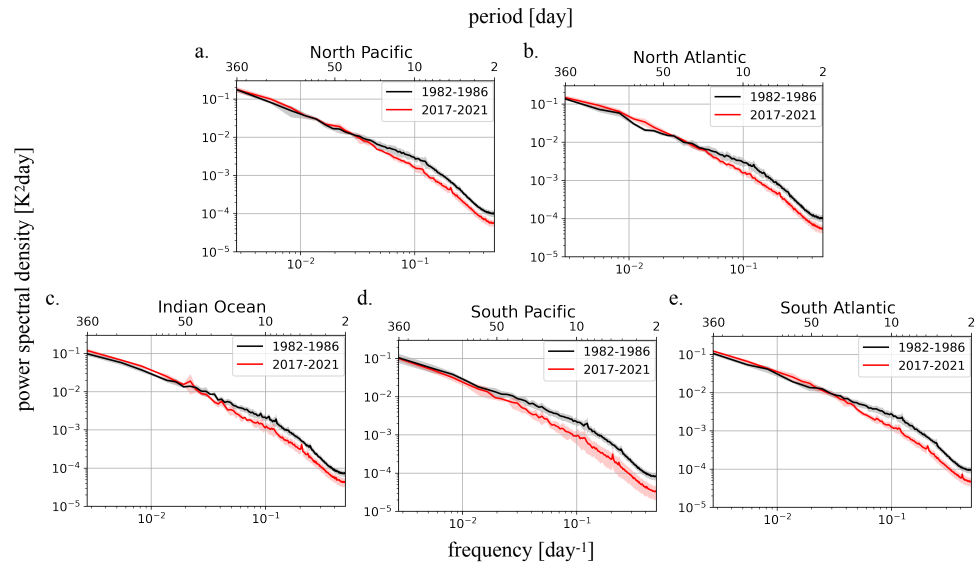

Fig. 2 Power spectral density (PSD) of the SST anomalies for five regions indicated by black boxes in Fig. 1a The averaged PSDs for the first and last five years of the analyzed period are shown by black and red lines, respectively, with shading representing one standard deviation.

in the tropical Pacific and Atlantic, exceeding 5 days per decade. In lower latitudes, between 20°S and 20°N, the average trend is roughly 2 days per decade, implying a doubling of the memory timescale over the last 40 years. Middle and high latitudes are also experiencing an increasing trend. For example, in the North Pacific, the SST memory timescale has been increasing at a rate of 2 days per decade, a full 50% increase over the last 40 years. The elongation of the daily SST memory timescale is evident from the autocorrelation analysis of SST anomalies alone (See Methods), emphasizing the robustness of this signal. This rising trend in the global ocean is likely linked to the observed increase in the duration of MHWs which have extended by more than 30 days in roughly 80% of the global ocean from 1982 to 2021 (Fig. 1c, Oliver et al. (2018)). These findings underscore a notable and concerning shift in the ocean's behaviour, allowing extreme SST anomalies to persist for much longer periods over the last four decades, potentially posing a greater threat to marine ecosystems.

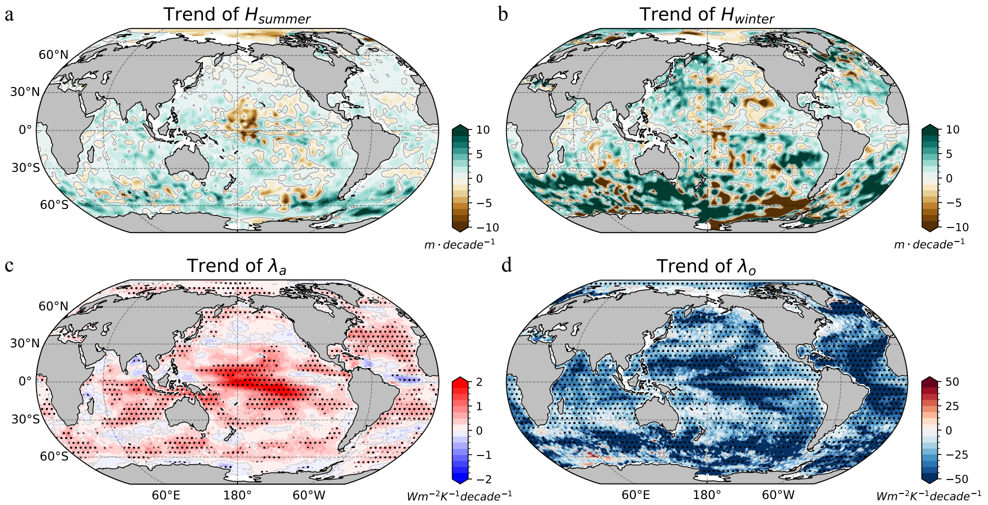

Fig. 3 **a-b**. The linear trend of the summertime and wintertime mixed layer depth (H_{summer} and H_{winter}) spanning from 1970 to 2018 (Sallée et al., 2021). **c-d**. The linear trend in atmospheric (λ_a) and oceanic (λ_o) damping coefficients from 1982 to 2021. Dotted regions in both **c** and **d** have statistically significant trends at a 95% confidence level.

Power spectrum analysis corroborates the extension of the daily SST memory timescales across the major ocean basins. Comparing the first five years (black lines in Fig. 2) with the last five years (red lines in Fig. 2), we see two notable changes over the past four decades. Variance at higher frequencies (red noise range) was reduced during the 2018-2021 period compared to 1982-1986, a statistically significant signature across all major ocean basins. In contrast, there was a slight increase in power at lower frequencies (white noise range) in the last five years. These shifts lead to an intersection of black and red lines in the 50-100 day range (Fig. 2). The diminished variance at high frequencies, coupled with heightened variance at low frequencies, implies extended SST memory timescales as is evident in changes in the autocorrelation coefficient.

Mechanisms behind the prolongation of SST memory

The global trend of increasing SST memory timescale has been investigated by employing a simple thermodynamic balance rooted in the AR(1) model, which accounts for both atmospheric and oceanic processes (see Methods). Changes in SST memory timescale can occur through two primary mechanisms: an increase in the heat capacity of the mixed layer and/or a decrease in the damping rates. The deepening of the mixed layer and concomitant heat capacity, reduces variance of SST anomalies at high frequencies (red noise range). Conversely, a decreasing trend in damping results in increased variance at low frequencies (white noise range). The observed SST Power Spectral Density (PSD) shows each of these changes, suggesting that both are contributing to changing SST memory timescale.

Recent findings reveal that, counter-intuitively, an increase in MLD is occurring concurrently with a strengthening of upper ocean stratification (Sallée et al., 2021). This deepening trend in the summertime is statistically significant, with a magnitude of 5-10 m per decade (Fig. 3a). During wintertime, the MLD and hence the heat capacity within it, exhibits an even more pronounced trend in the Southern Hemisphere (Fig. 3b). Assuming SST is representative of the mixed layer's temperature, this increased heat capacity implies a slower SST decay rate and hence reduced power at high frequency ranges, in accord with shifts in SST PSD reported here across all major ocean basins (Fig. 2).

Another contributing factor to the increased SST memory timescale is a decreasing damping coefficient, which, according to the AR(1) model, amplifies power at low frequencies. While our analysis is limited to timescales shorter than 365 days and does not fully resolve the white noise signal region, PSD consistently exhibits a trend towards increased variance at lower frequencies, except in the South Pacific (Fig. 2). This suggests that the damping coefficient has decreased in recent years and so contributed to the prolongation of SST memory timescale.

The damping coefficient can be decomposed into two distinct components, one associated with the atmosphere, the other the ocean. The atmospheric damping coefficient (λ_a) can be derived through differentiation of the bulk formulae with respect

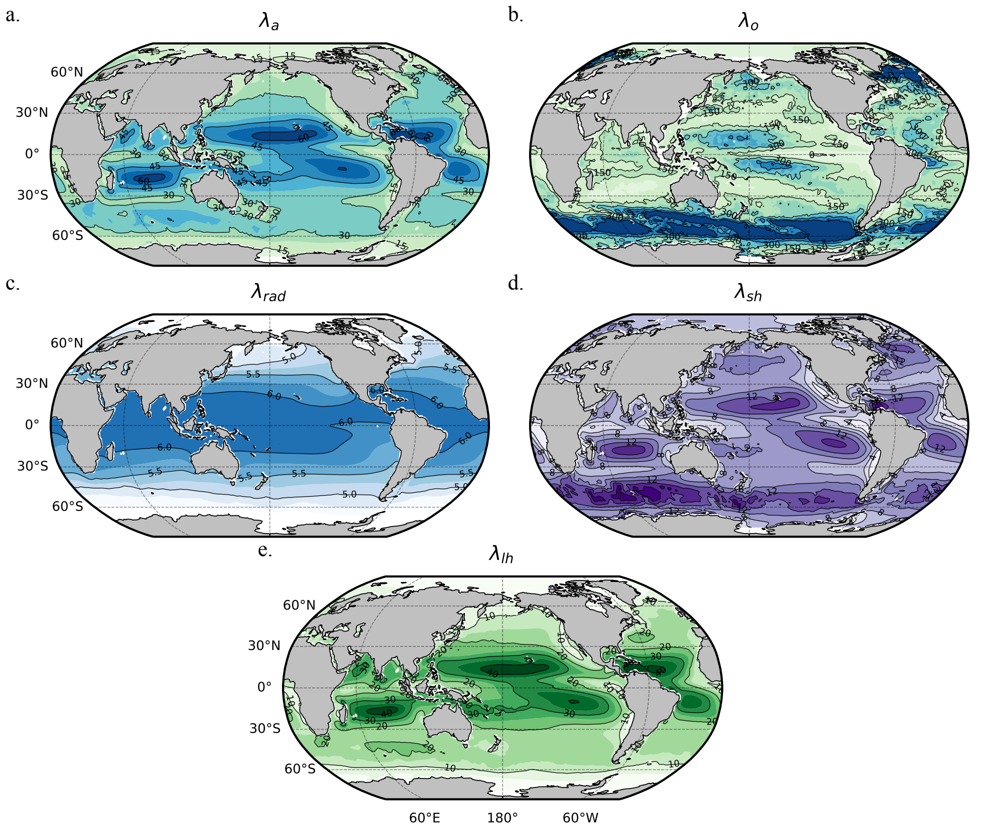

Fig. 4 **a, b**. Mean atmospheric (λ_a) and mean oceanic (λ_o) damping coefficient over the last 40 years. The atmospheric damping coefficient is decomposed into three contributions: **c**. long-wave radiation (λ_{rad}), **d**. sensible heat flux (λ_{sh}), and **e**. latent heat flux (λ_{lh}). The unit is W m^{-2} K^{-1}.

to SST (Klinger and Haine, 2019), revealing contributions from longwave, latent and sensible fluxes (see Methods). Using atmospheric ERA5 reanalysis data, and consistent with previous studies that employed lagged covariance methods between surface heat flux anomalies and SST anomalies (Frankignoul and Kestenare, 2002; Hausmann et al., 2016; Patrizio and Thompson, 2022), we find λ_a of roughly 30 W m^{-2} K^{-1} in the middle latitudes (Fig. 4a), with the latent heat flux as the largest contributor (Fig. 4e). This effect is particularly pronounced in subtropical gyre regions where evaporation exceeds precipitation. Meanwhile, in areas poleward of 30°, the influence of sensible heat flux tends to exceed that of both latent and longwave fluxes (Fig. 4d).

The atmospheric damping coefficient has a positive trend in many global ocean regions over the past 40 years (Fig. 3c). This is most prominent in the tropical Pacific, Indian Ocean, and extratropical Atlantic. This would lead to a shortening of the SST memory timescale due to the air-sea heat flux, in contrast to the observed prolongation of SST memory. While a few regions do show a negative atmospheric damping trend, this is relatively modest at roughly 0.5 W m^{-2} $decade^{-1}$, equivalent to an increase of 2 W m^{-2} in heat loss for a 1°C increase in SST over the past 40 years. Therefore, it is unlikely that surface heat fluxes can account for increased SST memory.

The oceanic damping coefficient (λ_o) plays a crucial role in modulating SST anomalies, exhibiting values which are larger than those of the atmosphere in specific regions (Patrizio and Thompson, 2022). It encapsulates many processes such as lateral mixing, vertical entrainment, and advection by ocean currents (Hausmann et al., 2016; Patrizio and Thompson, 2022). While it can be estimated using lagged covariance, analogously to the atmospheric damping coefficient (Patrizio and Thompson, 2022), here we compute it as a residual by subtracting the atmospheric damping coefficient from the total estimated from satellite SST and climatological MLD (see Methods). The resulting oceanic damping coefficients exceeds that of the atmosphere, and reveals elevated values in the Southern Ocean and the northern North Atlantic (Fig. 4b), consistent with previous studies (Patrizio and Thompson, 2022).

The trend in the ocean damping coefficient is found to be predominantly negative across almost all global oceans (Fig. 3d). This is consistent with an increased variance of SST anomalies in the low-frequency range (Fig. 2), as the solution of an AR(1)-model suggests (See Methods). This reduction in the oceanic damping coefficient is congruent with the strengthened upper ocean stratification trend, as measured by the buoyancy frequency at the pycnocline, observed across the global ocean (Sallée et al., 2021). With an intensification of upper ocean stratification, the exchange between the mixed layer and pycnocline requires more energy, resulting in an anticipated longer time for temperature anomalies in the mixed layer to decay. Consequently, the observed trends in the upper ocean, including the deepening of the mixed layer and the enhanced pycnocline stratification, are the major contributors to reducing SST anomaly decay rates, extending the memory timescales.

Discussion

The ocean plays a pivotal role in Earth's energy balance, storing over 90% of the excess heat in the Earth's system (Rhein et al., 2013; Trenberth et al., 2014; Von Schuckmann et al., 2023). This underscores the critical role of processes involved in absorbing excess heat from the atmosphere and transporting it into the deeper ocean. Over the past four decades, the observed lengthening of SST memory timescale, or the deceleration in the rate at which SST anomalies decay, suggests that the ocean has become less effective at absorbing excess heat from the atmosphere. The reduction in the ocean's damping coefficient reflects a decreased efficiency in heat transport from the mixed layer into the underlying ocean. This change can be attributed to the observed strengthening of upper ocean stratification (Sallée et al., 2021).

If stronger upper ocean stratification accelerates as the ocean warms (Kwiatkowski et al., 2020), we might expect to observe further decreases in the oceanic damping coefficient and hence a decrease in the efficiency of heat transfer into the deeper ocean. This, in turn, will pose an increased threat to marine organisms due to prolonged exposure to extreme near surface temperatures. Conversely, the potential future scenario of a shallower mixed layer, while less certain (Kwiatkowski et al., 2020), may amplify the variance of rapidly oscillating components of SST anomalies. This anticipated change could lead to a shorter SST memory timescale by allowing for increased variance in the high-frequency range. These opposing expectations and conflicting forecasts of SST persistence in prior studies (Li and Thompson, 2021; Shi et al., 2022) underscore the dependence of future SST memory timescale projections on the specific timescales considered. This study reveals how the surface ocean has evolved into a state which sustains anomalies for longer periods. This highlights the need for a comprehensive examination of SST memory timescales, encompassing daily, monthly, and annual scales, to ensure accurate predictions of the ocean's heat storage under a warming climate.

Methods

Data sources

This study makes use of four variables: sea surface temperature (SST), 2 m air temperature, 10 m wind and mixed layer depth (MLD). SST data is obtained from the Daily Optimum Interpolation Sea Surface Temperature version 2.0 and 2.1 (DOISST v2.0, v2.1) dataset (Reynolds et al., 2007; Banzon et al., 2016; Huang et al., 2021) provided by the National Centers for Environmental Information (NCEI). SST anomalies are then computed by subtracting both the seasonal cycle and the 40-year linear trend from the SST. The 2 m atmospheric temperature and 10 m wind, essential for calculating the heat flux feedback rate (detailed in the Methods section 'Changes in heat flux feedback rate'), are from the European Centre for Medium-Range Weather Forecasts (ECMWF) Reanalysis V5 (ERA5) dataset (Hersbach et al., 2020). Monthly mean MLD and the linear trend are obtained from Sallée et al. (2021). This dataset compiles over three million profiles from ship-based CTD data, Argo floats, and sensors attached to marine mammals, providing a 0.5-degree resolution MLD determined based on the density criteria. These variables are projected on a 1 degree regular grid with a daily timescale.

The study period spans 40 years from 1982 to 2021, encompassing the period of overlap between DOISST and ERA5. Although DOISST provides SST data from September 1981, we exclude this year due to incomplete coverage of a full calendar year. For the same reason, the year 2023 is not considered in the analysis. Exclusion of the year 2022 in our analysis stems from its relatively low variability (a red solid line in Fig. E1) and a sudden spike in the SST memory timescale (Fig. E2). Importantly including the year 2022 does not alter our conclusions (Fig. E5-E8) as the trend.

The trend of the SST memory timescale is estimated by the Theil-Sen estimator (Sen, 1968; Theil, 1992) (95% interval of the sampled slope), an unbiased metric that is a much less sensitive to outliers. Then the Mann-Kendall rank test (95% interval of the significance level) is employed to determine the significance of the trend (Mann, 1945; Kendall, 1948; Gilbert, 1987; Hussain and Mahmud, 2019).

Estimation of Surface thermal memory timescale

AR(1) model

Nonseasonal SST variabilities are often examined using a simplified model where SST anomalies evolve due to stochastic atmospheric forcing and damping mechanisms associated with SST anomalies (e.g. Hasselmann, 1976; Frankignoul and Hasselmann, 1977; Marshall and Plumb, 2008). Assuming a uniform mixed layer depth, this model can be written as

$$C_0 \frac{dT'}{dt} = F - \lambda T', \qquad (1)$$

where $C_0 = \rho c_p H$ is the heat capacity of the mixed layer, with ρ representing ocean density, c_p as the specific heat, and H as the mixed layer depth. In (1), F and λ respectively represent the stochastic forcing and damping rate of SST anomalies. The terms in the right-hand side can encompass not only atmospheric but also oceanic dynamic processes, such as temperature advection by both wind-driven gyre and Ekman current (Patrizio and Thompson, 2022).

The iterative solution to (1) is given by

$$T'(t) = T'(t - \delta t) \exp\left(-\frac{\lambda}{C_0}\delta t\right) + \int_{t-\delta t}^{t} \exp\left(\frac{\lambda}{C_0}(t' - t)\right) \frac{F(t')}{C_0} dt'. \tag{2}$$

The first and second terms in the right-hand side represent the exponential decay of the SST anomaly and the accumulated effects of stochastic forcing on the SST anomaly during $t - \delta t$ and t, respectively. The decay rate of SST anomaly can be characterized by a memory timescale ($\tau = C_0/\lambda$) This is essentially identical to the AR(1) model

$$T'_n = \phi T'_{n-1} + \epsilon_n, \tag{3}$$

where the subscripts denote the time step, ϕ is the lag-1 autocorrelation coefficient, and ϵ_n is the white noise forcing (Box et al., 1994; Bhattacharya and Burman, 2016). Thus, the memory timescale τ can be obtained from the lag-1 autocorrelation coefficient ϕ by relating the first terms of (3) and (2) and using a daily time interval ($\delta t = 1$ day)

$$\tau = \frac{C_0}{\lambda} = -\frac{1}{\ln \phi}. \tag{4}$$

The lag-1 autocorrelation coefficient ϕ is calculated using year-long SST anomalies for each year from 1982 to 2021.

Arctangent regressive model

While the AR(1) model effectively captures the processes controlling SST anomalies, the e-folding timescale is determined solely by the lag-1 correlation coefficient. Typically, this timescale is marked by the point where the autocorrelation falls below

$1/e$. An alternative approach involves the direct estimation of the surface thermal memory timescale from the autocorrelation of year-long SST anomalies. Given the discrete nature of the autocorrelation coefficient of daily SST anomalies, we first fit the autocorrelation using the following arctangent function:

$$\phi = 1 - \frac{\tan^{-1}(\alpha n)}{2}. \tag{5}$$

Here, ϕ is the autocorrelation coefficient, n is the lag value and α is the parameter that needs to be determined to minimize the root-mean-squared error of this arctangent function with respect to the autocorrelation. Then the memory timescale is found by identifying the point at which the autocorrelation coefficient becomes the $1/e$. With the memory timescale τ,

$$\begin{aligned} \frac{1}{e} &= 1 - \frac{\tan^{-1}(\alpha\tau)}{2} \\ \tau &= \frac{\tan(2 - 2/e)}{\alpha}. \end{aligned} \tag{6}$$

In the estimation of τ, one can vary the number of lag values (n) to fit the autocorrelation using (5). The 40-year mean τ and its trend, estimated by fitting (5) to the lag-1 autocorrelation, show similar results with those obtained from the AR(1) model (Fig. 1a-b, E3a and E4a). A higher value of n tends to increase the 40-year mean τ, notably in the eastern North Pacific, North Atlantic, and western South Pacific, although the spatial patterns remain comparable with the memory timescale of the SST anomalies estimated using the AR(1) model (Fig. E3b-e). Moreover, the trends in memory timescale estimated using (5) show a consistent tendency of elongated memory timescale globally, regardless n (Fig. E4b-e). These results suggest that the extended SST memory timescale is a robust signal.

Spectral analysis of SST anomalies

The spectral density of SST anomalies can be useful in diagnosing the changes in the observed SST memory timescale. As shown in Marshall and Plumb (2008), the solution for the SST anomalies in (1) takes the form of

$$T' = \mathrm{Re}(\hat{T'}_\omega \exp(i\omega t)), \tag{7}$$

where $\hat{T'}_\omega$ is the amplitude of the SST anomalies at frequency ω, and $\mathrm{Re}(\cdot)$ denotes the real part. Substituting (7) into (1) and taking the product with its conjugate yields the amplitude of SST anomalies as

$$\left(\hat{T}'_\omega\right)^2 = \left(\frac{\hat{F}_\omega}{C_0}\right)^2 \frac{1}{\omega^2 + \omega_c^2}, \tag{8}$$

where $\hat{F}_\omega$ is the amplitude of the stochastic heat exchange between atmosphere and ocean at ω and $\omega_c = \lambda / C_0 = (\tau)^{-1}$.

The spectral density of SST anomalies shows two distinct characteristics of $\hat{T}'_\omega$, exhibiting both 'red' and 'white' noise features, depending on ω relative to ω_c. At high frequencies ($\omega \gg \omega_c$), the amplitude $\hat{T}'_\omega$ can be approximated by $\hat{F}_\omega / (C_0 \omega)$. This approximation implies a decline in SST anomaly variability with frequency, yielding a 'red noise' power spectrum. In this regime, changes in C_0 can shift the power density spectrum of SST anomalies upward or downward with no significant changes in $\hat{F}_\omega$. Specifically, an increase of C_0 can lower the $\hat{T}'_\omega$, indicating that the deepening of the mixed layer and the subsequent increase in its heat content can reduce the variability of the SST anomalies at the frequency greater than ω_c, aligning with observational findings (Fig. 2 and 3ab).

At low frequencies ($\omega \ll \omega_c$), the amplitude $\hat{T}'_\omega$ can be approximated by $\tau \hat{F}_\omega / C_0$ (or $\hat{F}_\omega/\lambda$), leading to a frequency-independent 'white' noise response. In this range, the negative feedback, represented by the damping rate λ, plays a critical role in subsiding the SST anomalies. A decrease in λ, with minimal changes in $\hat{F}\omega$ can elevate $\hat{T}'_\omega$, consistent with the observed tendency (Fig. 2), indicating that a less effective negative feedback can prolong SST anomalies. Additionally, it can shift the critical frequency, ω_c, to lower frequencies, expanding the 'red' noise region. Hence, the examination of the power spectral density of the SST anomalies offers a credible explanation for the increasing trend observed in the SST memory timescale.

Estimation of damping coefficient

The damping coefficient λ in (1), can be partitioned into two components: the rate of damping through surface heat flux (λ_a) and through oceanic processes (λ_o). λ_a is further decomposed into three contributions: λ_{rad}, λ_{sh} and λ_{lh} associated with long-wave radiation (Q_B), sensible heat flux (Q_H), and latent heat flux (Q_L), respectively (Klinger and Haine, 2019).

$$\begin{aligned} \lambda_a &= \lambda_{rad} + \lambda_{sh} + \lambda_{lh} \\ &= \left(\frac{\partial Q_B}{\partial T} + \frac{\partial Q_H}{\partial T} + \frac{\partial Q_L}{\partial T} \right) \bigg|_{T=T_A}, \end{aligned} \tag{9}$$

where T_A is the atmospheric temperature at 2 m obtained from ERA5.

The terms in (9) are estimated by linearizing the bulk formulas (Roll, 1965; Large and Yeager, 2004) as follows (Hausmann et al., 2017; Yang et al., 2018; Yuan et al., 2022):

$$\frac{\partial Q_B}{\partial T} = 4\sigma T^3, \tag{10}$$
$$\frac{\partial Q_H}{\partial T} = \rho_a c_p C_H U, \tag{11}$$
$$\frac{\partial Q_L}{\partial T} = -\Lambda_v C_E U \frac{q_1 q_2}{T^2} \exp(\frac{q_2}{T}). \tag{12}$$

The names, units and values of the variables and parameters in (10)-(12) are adapted from Large and Yeager (2004) and listed in Table 1.

symbol	name	units	value
σ	Stefan-Boltzmann coefficient	W m^{-2} K^{-4}	5.67×10^{-8}
ρ_a	surface air density	kg m^{-3}	1.22
c_p	specific heat of the air	J kg^{-1} K^{-1}	1000.5
Λ_v	latent heat of vaporization	J kg^{-1}	2.5×10^6
U	10 m wind speed	m s^{-1}	ERA5
T	2 m atmospheric temperature	K	ERA5
C_H	transfer coefficient for sensible heat	Dimensionless	$f(U)$
C_E	transfer coefficient for evaporation	Dimensionless	$g(U)$
q_1	-	kg m^{-3}	0.98×640380
q_2	-	K	-5107.4

Table 1 Names, units, and values of the variables and parameters appeared in (10)-(12).

λ_a is estimated daily, and its trend is computed from 1982 to 2021. Subsequently, λ_o, the damping coefficient associated with oceanic processes is simply computed as the residual of λ and λ_a:

$$\lambda_o = \lambda - \lambda_a. \tag{13}$$

Data availability. Details regarding the source database utilized in this study can be found at the following URLs: https://doi.org/10.5067/GHAAO-4BC21 and https://doi.org/10.24381/cds.adbb2d47. The global maps illustrating trend and climatology MLD fields, as discussed in this paper, are accessible at https://doi.org/10.1038/s41586-021-03303-x.

Code availability. The analytical code employed for the results and Supplementary Information in this paper can be accessed at https://github.com/ChaehyeongLee/ThermalMemory.git.

Acknowledgments. This study was supported by a National Research Foundation of Korea (NRF) grant funded by the Korean government (MSIT) (2018R1A5A1024958 and 2022R1A2C1009792). JM was supported by the Physical Oceanography program of NASA and the MIT-GISS cooperative agreement.

Author contributions. H.S. designed the study; C.L. and H.S. performed the analysis. C.L. created figures. Y.C., A.C. and J.M. helped in the investigation. C.L. wrote the original draft; and C.L., H.S, Y.C and J.M reviewed and edited the paper.

Competing interests. The authors declare no competing interests.

Extended data figures and tables.

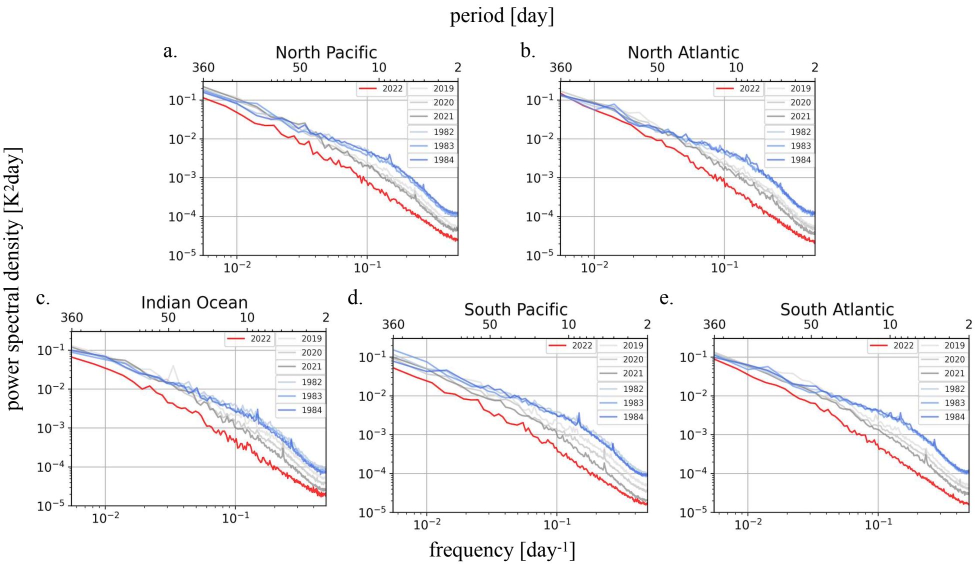

Fig. E1 a-e. PSD of annual SST anomalies for five regions, denoted by white boxes in Fig. 1a, during two different time periods: 1982-1984 (greys) and 2019-2021 (blues). The PSD of SST anomalies for the year of 2022 is shown as a red solid line.

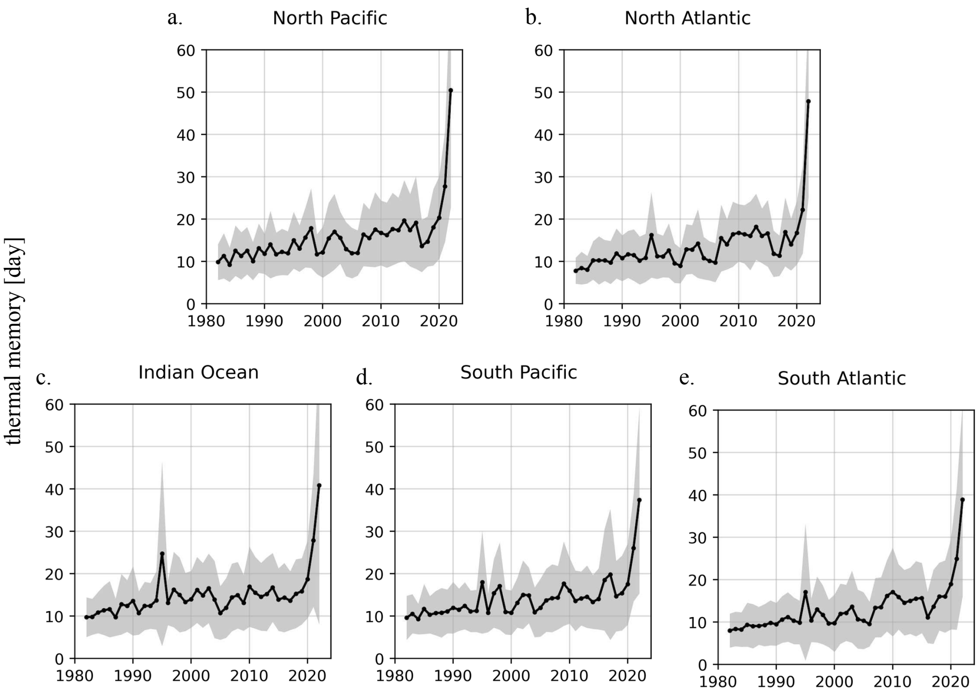

Fig. E2 Annual variation of the thermal memory across five regions from 1982 to 2022. Shading represents one standard deviation.

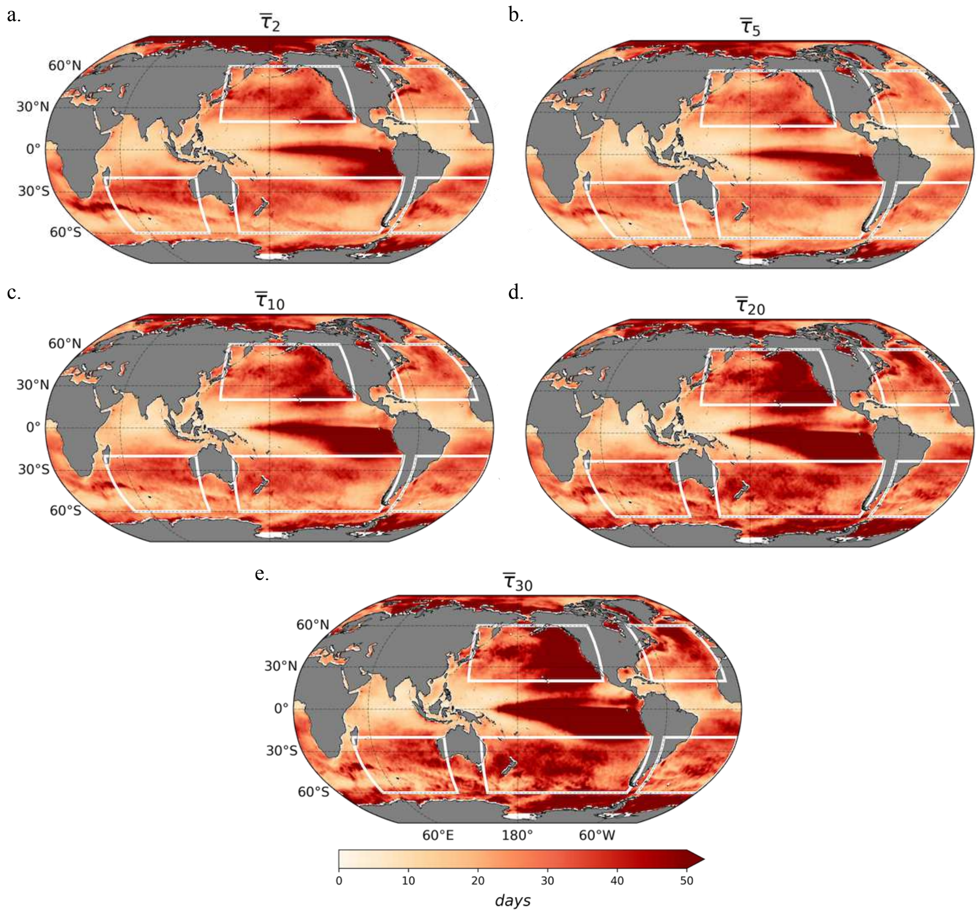

Fig. E3 a-e. The mean memory timescales ($\overline{\tau}$) of SST anomalies over a 40-year period (1982-2021). Optimal coefficients for the arctangent function are determined using 2, 5, 10, 20, and 30 consecutive autocorrelation coefficients of SST anomalies, spanning from the 0-lag to the lag $(n-1)$.

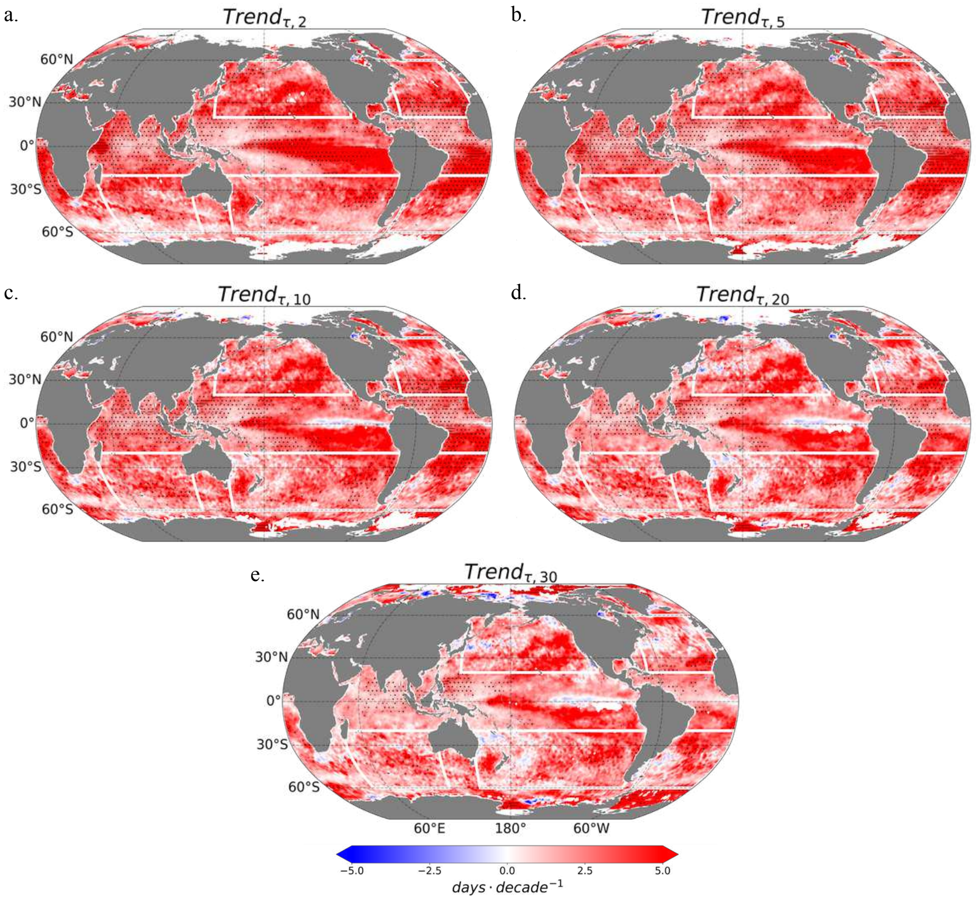

Fig. E4 a-e. The linear trend of the memory timescale, which is calculated using the arctangent model depicted in Extended Data Fig. E3a-e. from 1982 to 2021, respectively. The dotted and dashed areas represent the regions where τ in 2021 has increased by 50-100% and over 100% compared to 1982, respectively.

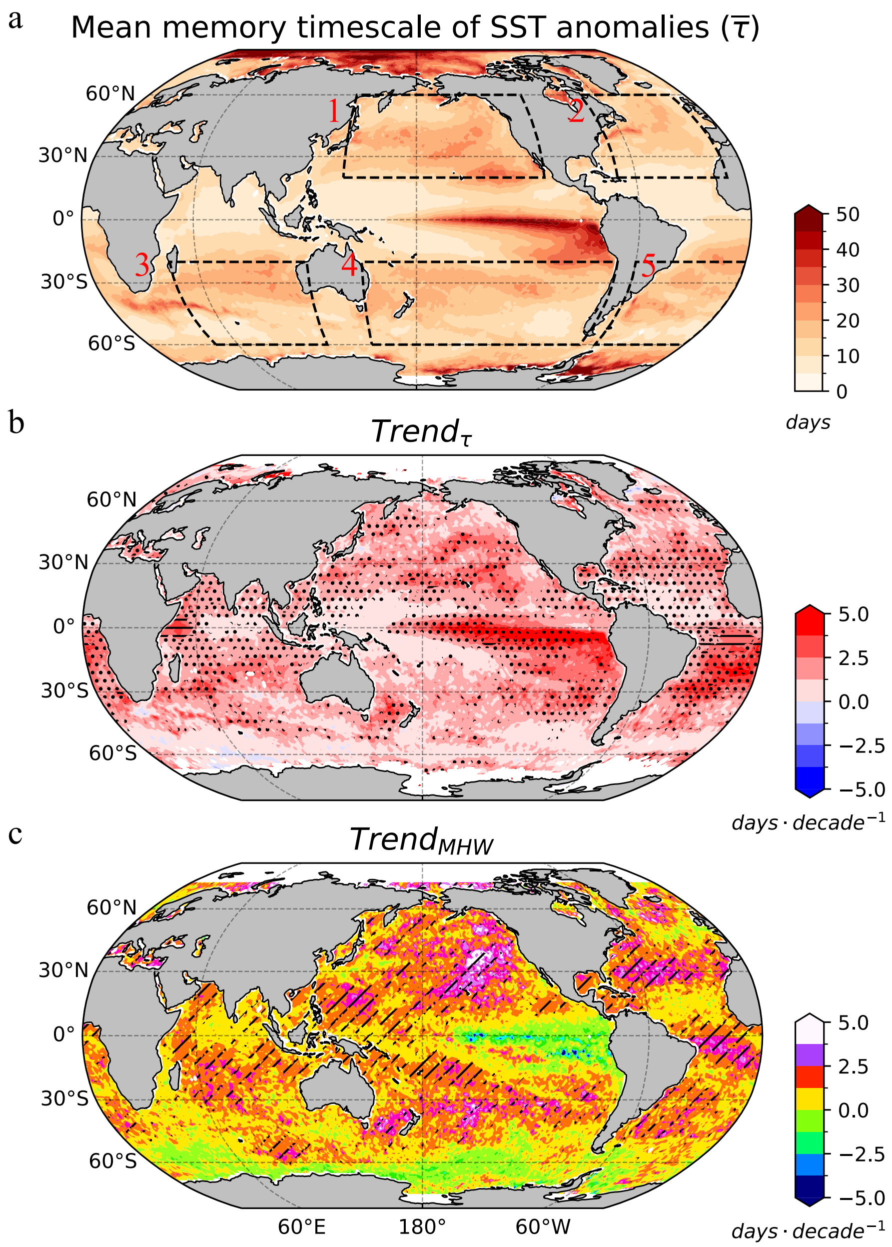

Fig. E5 The year of 2022 is considered. **a**. The mean memory timescale of the SST anomalies ($\overline{\tau}$) estimated from the observation. **b**. The linear trend from 1982 to 2022. The white boxes indicate the regions of interest where the energy spectra of the SST anomalies were calculated. The dotted and dashed areas in b represent the regions where τ in 2022 has increased by 50-100% and over 100% compared to 1982, respectively. Note that nearly every region globally exhibits a statistically significant increasing trend. **c**. Linear trend in marine heatwave duration from 1982 to 2022. The dashed areas in **c** represent the regions in which trends in marine heatwaves duration are statistically significant at the 95% confidence level.

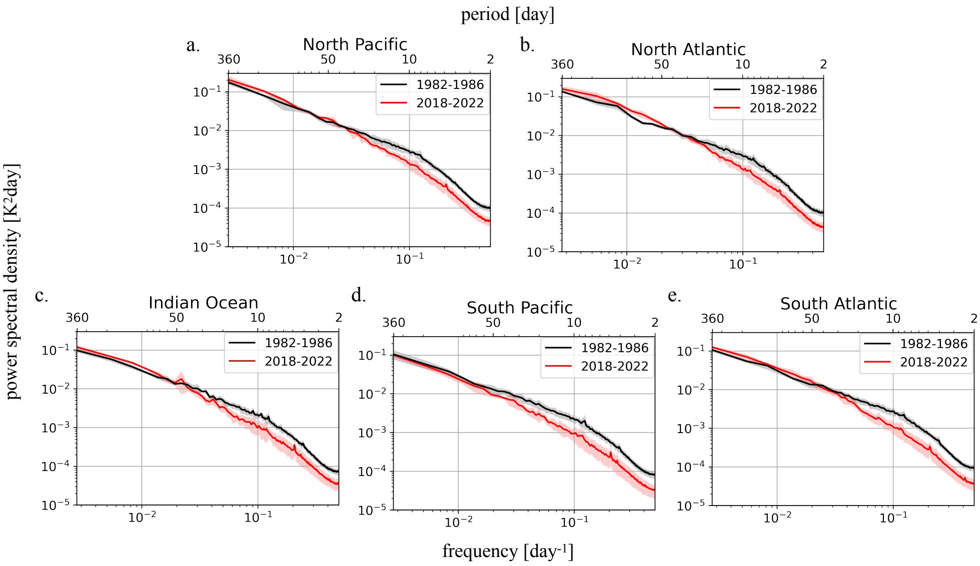

Fig. E6 The year of 2022 is considered. PSD of the SST anomalies for five regions indicated by white boxes in Extended Data Fig. E5. The averaged PSD for the first and last five years of the analysed period is shown by black and red lines, respectively, with shading representing one standard deviation.

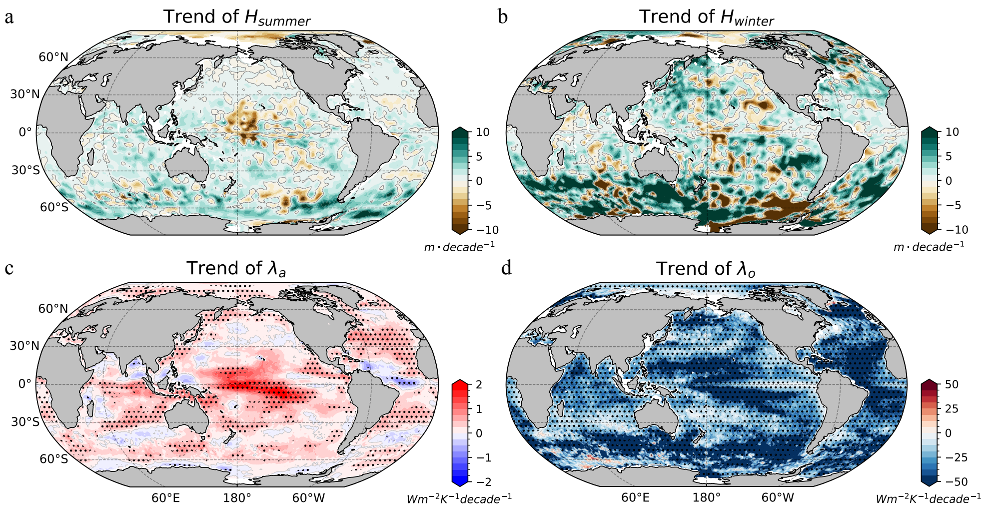

Fig. E7 The year of 2022 is considered. a-b. The linear trend of the summertime and wintertime mixed layer depth spanning from 1970 to 2018 (Sallée et al., 2021). **c**. The linear trend in total surface λ_a, and in λ_o associated with the oceanic processes from 1982 to 2022. Dotted regions in both **c** and **d** have statistically significant trends at a 95% confidence level.

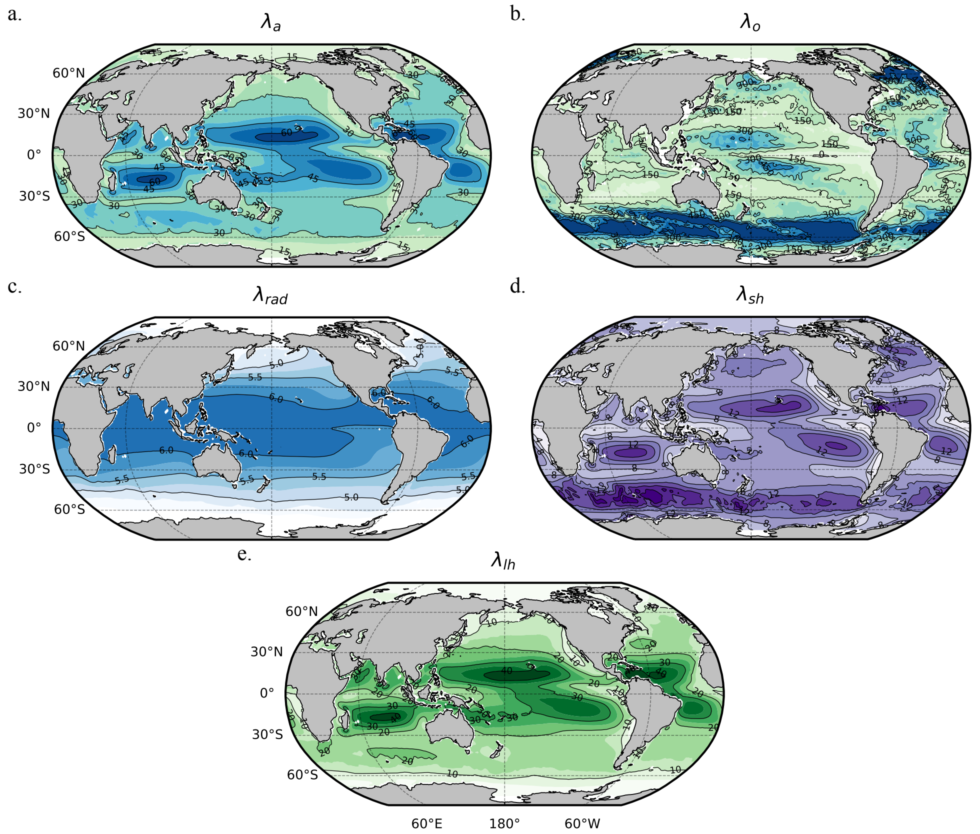

Fig. E8 The year of 2022 is considered. **a-b**. Mean atmospheric damping coefficient (λ_a) and mean damping coefficient (λ_o) attributed to oceanic interior processes over the last 41 years. The atmospheric damping coefficient is decomposed into three contributions: **c**. long-wave radiation (λ_{rad}), **d**. sensible heat flux (λ_{sh}), and **e**. latent heat flux (λ_{lh}).

References

Frankignoul, C., Hasselmann, K.: Stochastic climate models, Part II Application to sea-surface temperature anomalies and thermocline variability. Tellus A: Dynamic Meteorology and Oceanography **29**(4), 289–305 (1977) https://doi.org/10.3402/TELLUSA.V29I4.11362

Deser, C., Alexander, M.A., Xie, S.-P., Phillips, A.S.: Sea surface temperature variability: Patterns and mechanisms. Annual Review of Marine Science **2**, 115–143 (2010) https://doi.org/10.1146/annurev-marine-120408-151453

Xie, S.-P.: A Dynamic Ocean–Atmosphere Model of the Tropical Atlantic Decadal Variability. Journal of Climate **12**(1), 64–70 (1999) https://doi.org/10.1175/1520-0442(1999)012⟨0064:ADOAMO⟩2.0.CO;2

Frölicher, T.L., Laufkötter, C.: Emerging risks from marine heat waves. Nature Communications **9**(1), 650 (2018) https://doi.org/10.1038/S41467-018-03163-6

Mills, K.E., Pershing, A.J., Brown, C.J., Chen, Y., Chiang, F.S., Holland, D.S., Lehuta, S., Nye, J.A., Sun, J.C., Thomas, A.C., Wahle, R.A.: Fisheries management in a changing climate: Lessons from the 2012 ocean heat wave in the Northwest Atlantic. Oceanography **26**(2), 191–195 (2013) https://doi.org/10.5670/OCEANOG.2013.27

Moore, J.A.Y., Bellchambers, L.M., Depczynski, M.R., Evans, R.D., Evans, S.N., Field, S.N., Friedman, K.J., Gilmour, J.P., Holmes, T.H., Middlebrook, R., Radford, B.T., Ridgway, T., Shedrawi, G., Taylor, H., Thomson, D.P., Wilson, S.K.: Unprecedented Mass Bleaching and Loss of Coral across 12° of Latitude in Western Australia in 2010–11. PLoS one **7**(12), 51807 (2012) https://doi.org/10.1371/JOURNAL.PONE.0051807

Rhein, M., Rintoul, S.R., Aoki, S., Campos, E., Chambers, D., Feely, R.A., Gulev, S., Johnson, G.C., Josey, S.A., Kostianoy, A., Mauritzen, C., Roemmich, D., Talley, L.D., Wang, F.: Observations: Ocean. In: Stocker, T.F., Qin, D., Plattner, G.-K., Tignor, M., Allen, S.K., Boschung, J., Nauels, A., Xia, Y., Bex, V., Midgley, P.M. (eds.) Climate Change 2013: The Physical Science Basis. Contribution of Working Group I to the Fifth Assessment Report of the Intergovernmental Panel on Climate Change, pp. 255–316. Cambridge University Press, Cambridge, United Kingdom and New York, NY, USA (2013)

Trenberth, K.E., Fasullo, J.T., Balmaseda, M.A.: Earth's Energy Imbalance. Journal of Climate **27**(9), 3129–3144 (2014) https://doi.org/10.1175/JCLI-D-13-00294.1

Von Schuckmann, K., Minière, A., Gues, F., Cuesta-Valero, F.J., Kirchengast, G., Adusumilli, S., Straneo, F., Ablain, M., Allan, R.P., Barker, P.M., Beltrami, H., Blazquez, A., Boyer, T., Cheng, L., Church, J., Desbruyeres, D., Dolman, H., Domingues, C.M., García-García, A., Giglio, D., Gilson, J.E., Gorfer, M., Haimberger, L., Hakuba, M.Z., Hendricks, S., Hosoda, S., Johnson, G.C., Killick, R., King, B., Kolodziejczyk, N., Korosov, A., Krinner, G., Kuusela, M., Landerer, F.W., Langer, M., Lavergne, T., Lawrence, I., Li, Y., Lyman, J., Marti, F., Marzeion, B., Mayer, M., MacDougall, A.H., McDougall, T., Monselesan, D.P., Nitzbon, J., Otosaka, I., Peng, J., Purkey, S., Roemmich, D., Sato, K., Sato, K., Savita, A., Schweiger, A., Shepherd, A., Seneviratne, S.I., Simons, L., Slater, D.A., Slater, T., Steiner, A.K., Suga, T., Szekely, T., Thiery, W., Timmermans, M.-L., Vanderkelen, I., Wjiffels, S.E., Wu, T., Zemp, M.: Heat stored in the earth system 1960–2020: where does the energy go? Earth System Science Data **15**(4), 1675–1709 (2023) https://doi.org/10.5194/essd-15-1675-2023

Hasselmann, K.: Stochastic climate models Part I. Theory. Tellus **28**, 473–485 (1976) https://doi.org/10.1111/J.2153-3490.1976.TB00696.X

Marshall, J., Plumb, R.A.: Atmosphere, Ocean and Climate Dynamics: An Introductory Text, pp. 262–266. Elsevier, Amsterdam (2008)

Boulton, C.A., Lenton, T.M.: Slowing down of North Pacific climate variability and its implications for abrupt ecosystem change. Proceedings of the National Academy of Sciences of the United States of America **112**(37), 11496–11501 (2015) https://doi.org/10.1073/pnas.1501781112

Patrizio, C.R., Thompson, D.W.J.: Understanding the Role of Ocean Dynamics in Midlatitude Sea Surface Temperature Variability Using a Simple Stochastic Climate Model. Journal of Climate **35**(11), 3313–3333 (2022) https://doi.org/10.1175/JCLI-D-21-0184.1

Smale, D.A., Wernberg, T., Oliver, E.C.J., Thomsen, M., Harvey, B.P., Straub, S.C., Burrows, M.T., Alexander, L.V., Benthuysen, J.A., Donat, M.G., Feng, M., Hobday, A.J., Holbrook, N.J., Perkins-Kirkpatrick, S.E., Scannell, H.A., Gupta, A.S., Payne, B.L., Moore, P.J.: Marine heatwaves threaten global biodiversity and the provision of ecosystem services. Nature Climate Change **9**(4), 306–312 (2019) https://doi.org/10.1038/s41558-019-0412-1

Ding, R., Li, J.: Decadal and seasonal dependence of North Pacific sea surface temperature persistence. Journal of Geophysical Research: Atmospheres **114**(D1) (2009) https://doi.org/10.1029/2008JD010723

Lenton, T.M., Dakos, V., Bathiany, S., Scheffer, M.: Observed trends in the magnitude and persistence of monthly temperature variability. Scientific Reports **7**(1), 5940 (2017) https://doi.org/10.1038/s41598-017-06382-x

Shi, H., Jin, F.-F., Wills, R.C.J., Jacox, M.G., Amaya, D.J., Black, B.A., Rykaczewski, R.R., Bograd, S.J., García-Reyes, M., Sydeman, W.J.: Global decline in ocean memory over the 21st century. Science Advances **8**(18), 3468 (2022) https://doi.org/10.1126/sciadv.abm3468

Hobday, A.J., Alexander, L.V., Perkins, S.E., Smale, D.A., Straub, S.C., Oliver, E.C.J., Benthuysen, J.A., Burrows, M.T., Donat, M.G., Feng, M., Holbrook, N.J., Moore, P.J., Scannell, H.A., Sen Gupta, A., Wernberg, T.: A hierarchical approach to defining marine heatwaves. Progress in Oceanography **141**, 227–238 (2016) https://doi.org/10.1016/j.pocean.2015.12.014

Hobday, A.J., Oliver, E.C., Gupta, A.S., Benthuysen, J.A., Burrows, M.T., Donat, M.G., Holbrook, N.J., Moore, P.J., Thomsen, M.S., Wernberg, T., *et al.*: Categorizing and naming marine heatwaves. Oceanography **31**(2), 162–173 (2018) https://doi.org/10.5670/oceanog.2018.205

Oliver, E.C.J., Benthuysen, J.A., Darmaraki, S., Donat, M.G., Hobday, A.J., Holbrook, N.J., Schlegel, R.W., Sen Gupta, A.: Marine Heatwaves. Annual Review of Marine Science **13**(1), 313–342 (2021) https://doi.org/10.1146/annurev-marine-032720-095144

Botsford, L.W., Lawrence, C.A., Dever, E.P., Hastings, A., Largier, J.: Effects of variable winds on biological productivity on continental shelves in coastal upwelling systems. Deep Sea Research Part II: Topical Studies in Oceanography **53**(25), 3116–3140 (2006) https://doi.org/10.1016/j.dsr2.2006.07.011

García-Reyes, M., Largier, J.L., Sydeman, W.J.: Synoptic-scale upwelling indices and predictions of phyto- and zooplankton populations. Progress in Oceanography **120**, 177–188 (2014) https://doi.org/10.1016/J.POCEAN.2013.08.004

Aguirre, C., Garreaud, R.D., Rutllant, J.A.: Surface ocean response to synoptic-scale variability in wind stress and heat fluxes off south-central Chile. Dynamics of Atmospheres and Oceans **65**, 64–85 (2014) https://doi.org/10.1016/J.DYNATMOCE.2013.11.001

Aguirre, C., Rojas, M., Garreaud, R.D., Rahn, D.A.: Role of synoptic activity on projected changes in upwelling-favourable winds at the ocean's eastern boundaries. npj Climate and Atmospheric Science **2**(1), 44 (2019) https://doi.org/10.1038/s41612-019-0101-9

Dillon, M.E., Woods, H.A., Wang, G., Fey, S.B., Vasseur, D.A., Telemeco, R.S., Marshall, K., Pincebourde, S.: Life in the Frequency Domain: the Biological Impacts of Changes in Climate Variability at Multiple Time Scales. Integrative and Comparative Biology **56**(1), 14–30 (2016) https://doi.org/10.1093/icb/icw024

Bulgin, C.E., Merchant, C.J., Ferreira, D.: Tendencies, variability and persistence of sea surface temperature anomalies. Scientific Reports **10**(1), 7986 (2020) https://doi.org/10.1038/s41598-020-64785-9

Li, J., Thompson, D.W.J.: Widespread changes in surface temperature persistence under climate change. Nature **599**(7885), 425–430 (2021) https://doi.org/10.1038/s41586-021-03943-z

Reynolds, R.W., Smith, T.M., Liu, C., Chelton, D.B., Casey, K.S., Schlax, M.G.: Daily High-Resolution-Blended Analyses for Sea Surface Temperature. Journal of Climate **20**(22), 5473–5496 (2007) https://doi.org/10.1175/2007JCLI1824.1

Oliver, E.C.J., Donat, M.G., Burrows, M.T., Moore, P.J., Smale, D.A., Alexander, L.V., Benthuysen, J.A., Feng, M., Gupta, A.S., Hobday, A.J., Holbrook, N.J., Perkins-Kirkpatrick, S.E., Scannell, H.A., Straub, S.C., Wernberg, T.: Longer and more frequent marine heatwaves over the past century. Nature Communications

9(1), 1–12 (2018) https://doi.org/10.1038/s41467-018-03732-9

Sallée, J.B., Pellichero, V., Akhoudas, C., Pauthenet, E., Vignes, L., Schmidtko, S., Garabato, A.N., Sutherland, P., Kuusela, M.: Summertime increases in upper-ocean stratification and mixed-layer depth. Nature **591**(7851), 592–598 (2021) https://doi.org/10.1038/s41586-021-03303-x

Klinger, B.A., Haine, T.W.N.: Ocean Circulation in Three Dimensions, pp. 126–154. Cambridge University Press, Cambridge, England (2019). https://doi.org/10.1017/9781139015721

Frankignoul, C., Kestenare, E.: The surface heat flux feedback. Part I: Estimates from observations in the Atlantic and the North Pacific. Climate Dynamics **19**, 633–648 (2002) https://doi.org/10.1007/s00382-002-0252-x

Hausmann, U., Czaja, A., Marshall, J.: Estimates of Air–Sea Feedbacks on Sea Surface Temperature Anomalies in the Southern Ocean. Journal of Climate **29**(2), 439–454 (2016) https://doi.org/10.1175/JCLI-D-15-0015.1

Kwiatkowski, L., Torres, O., Bopp, L., Aumont, O., Chamberlain, M., Christian, J.R., Dunne, J.P., Gehlen, M., Ilyina, T., John, J.G., Lenton, A., Li, H., Lovenduski, N.S., Orr, J.C., Palmieri, J., Santana-Falcón, Y., Schwinger, J., Séférian, R., Stock, C.A., Tagliabue, A., Takano, Y., Tjiputra, J., Toyama, K., Tsujino, H., Watanabe, M., Yamamoto, A., Yool, A., Ziehn, T.: Twenty-first century ocean warming, acidification, deoxygenation, and upper-ocean nutrient and primary production decline from CMIP6 model projections. Biogeosciences **17**(13), 3439–3470 (2020) https://doi.org/10.5194/bg-17-3439-2020

Banzon, V., Smith, T.M., Chin, T.M., Liu, C., Hankins, W.: A long-term record of blended satellite and in situ sea-surface temperature for climate monitoring, modeling and environmental studies. Earth System Science Data **8**(1), 165–176 (2016) https://doi.org/10.5194/ESSD-8-165-2016

Huang, B., Liu, C., Banzon, V., Freeman, E., Graham, G., Hankins, B., Smith, T., Zhang, H.M.: Improvements of the Daily Optimum Interpolation Sea Surface Temperature (DOISST) Version 2.1. Journal of Climate **34**(8), 2923–2939 (2021) https://doi.org/10.1175/JCLI-D-20-0166.1

Hersbach, H., Bell, B., Berrisford, P., Hirahara, S., Horányi, A., Muñoz-Sabater, J., Nicolas, J., Peubey, C., Radu, R., Schepers, D., Simmons, A., Soci, C., Abdalla, S., Abellan, X., Balsamo, G., Bechtold, P., Biavati, G., Bidlot, J., Bonavita, M., De Chiara, G., Dahlgren, P., Dee, D., Diamantakis, M., Dragani, R., Flemming, J., Forbes, R., Fuentes, M., Geer, A., Haimberger, L., Healy, S., Hogan, R.J., Hólm, E., Janisková, M., Keeley, S., Laloyaux, P., Lopez, P., Lupu, C., Radnoti, G., Rosnay, P., Rozum, I., Vamborg, F., Villaume, S., Thépaut, J.N.: The ERA5 global reanalysis. Quarterly Journal of the Royal Meteorological Society **146**(730), 1999–2049 (2020) https://doi.org/10.1002/QJ.3803

Sen, P.K.: Estimates of the Regression Coefficient Based on Kendall's Tau. Journal of the American Statistical Association **63**(324), 1379–1389 (1968) https://doi.org/10.1080/01621459.1968.10480934

Theil, H.: In: Raj, B., Koerts, J. (eds.) A Rank-Invariant Method of Linear and Polynomial Regression Analysis, pp. 345–381. Springer, Dordrecht (1992). https://doi.org/10.1007/978-94-011-2546-8_20

Mann, H.B.: Nonparametric Tests Against Trend. Econometrica **13**(3), 245–259 (1945) https://doi.org/10.2307/1907187

Kendall, M.G.: Rank Correlation Methods. Griffin, Oxford, England (1948)

Gilbert, R.O.: Statistical Methods for Environmental Pollution Monitoring. John Wiley & Sons, New York, NY, USA (1987)

Hussain, M., Mahmud, I.: pyMannKendall: a python package for non parametric Mann Kendall family of trend tests. Journal of Open Source Software **4**(39), 1556 (2019) https://doi.org/10.21105/joss.01556

Box, G.E.P., Jenkins, G.M., Reinsel, G.C.: Time Series Analysis: Forcasting and Control, 3rd edn., pp. 46–59. Prentice Hall, Upper Saddle River, NJ, USA (1994)

Bhattacharya, P.K., Burman, P.: Theory and Methods of Statistics, 1st edn., pp. 431–489. Academic Press., Cambridge, MA, USA (2016). https://doi.org/10.1016/C2014-0-02379-9

Roll, H.U.: Physics of the Marine Atmosphere, p. 426. Academic Press, New York, NY, USA (1965)

Large, W.G., Yeager, S.G.: Diurnal to Decadal Global Forcing for Ocean and Sea-Ice Models: The Data Sets and Flux Climatologies. NCAR Tech. Note NCAR/TN-460+STR, National Center for Atmospheric Research, Boulder, CO, USA (2004)

Hausmann, U., Czaja, A., Marshall, J.: Mechanisms controlling the SST air-sea heat flux feedback and its dependence on spatial scale. Climate Dynamics **48**, 1297–1307 (2017) https://doi.org/10.1007/s00382-016-3142-3

Yang, P., Jing, Z., Wu, L.: An assessment of representation of oceanic mesoscale eddy-atmosphere interaction in the current generation of general circulation models and reanalyses. Geophysical Research Letters **45**(21), 11856–11865 (2018) https://doi.org/10.1029/2018GL080678

Yuan, M., Li, F., Ma, X., Yang, P.: Spatio-temporal variability of surface turbulent heat flux feedback for mesoscale sea surface temperature anomaly in the global ocean. Frontiers in Marine Science **9** (2022) https://doi.org/10.3389/fmars.2022.957796